

## Towards superconductivity in p-type delta-doped Si/Al/Si heterostructures

A. N. Ramanayaka,<sup>1,2</sup> Hyun-Soo Kim,<sup>1,2</sup> J. A. Hagmann,<sup>1</sup> R. E. Murray,<sup>1,2</sup> Ke Tang,<sup>1,2</sup> F. Meisenkothen,<sup>1</sup> H. R. Zhang,<sup>1,3</sup> L. A. Bendersky,<sup>1</sup> A. V. Davydov,<sup>1</sup> Neil M. Zimmerman,<sup>1</sup> C. A. Richter,<sup>1</sup> and J. M. Pomeroy<sup>1,a</sup>

<sup>1</sup>National Institute of Standards & Technology, Gaithersburg, Maryland 20899, USA

<sup>2</sup>Joint Quantum Institute, University of Maryland, College Park, Maryland 20742, USA

<sup>3</sup>Theiss Research, Inc., La Jolla, California 92037, USA

(Received 19 June 2018; accepted 19 July 2018; published online 30 July 2018)

In pursuit of superconductivity in p-type silicon (Si), we are using a single atomic layer of aluminum (Al) sandwiched between a Si substrate and a thin Si epi-layer. The delta layer was fabricated starting from an ultra high vacuum (UHV) flash anneal of Si(100) surface, followed by physical vapor deposition of Al monolayer. To activate the Al dopants, the sample was then annealed *in-situ* at 550 °C for 1 min. The Si capping layer was electron-beam evaporated *in-situ* at room temperature, followed by an *ex-situ* anneal at 550 °C for 10 min to recrystallize the Si capping layer. Low temperature magnetotransport measurements yield a maximum hole mobility of 20 cm<sup>2</sup>/V/s at a carrier density  $1.39 \times 10^{14}$  holes/cm<sup>2</sup>, which corresponds to  $\approx (0.93 \pm 0.1)$  holes per dopant atom. No superconductivity was observed in these devices even at  $T < 300$  mK. Atom probe tomography and energy-dispersive X-ray spectroscopy analyses suggest that the Al dopants become distributed over  $\approx (17$  to 25) nm thickness. Redistribution of Al dopants reduces Al atomic concentration in Si matrix below the critical density to observe superconductivity. © 2018 Author(s). All article content, except where otherwise noted, is licensed under a Creative Commons Attribution (CC BY) license (<http://creativecommons.org/licenses/by/4.0/>). <https://doi.org/10.1063/1.5045338>

Silicon is the workhorse material in the semiconductor industry due to the high quality oxides that can be grown and the desirable dopant chemistry for a variety of both n- and p-type dopants. While Si is predominantly used as a semiconductor, superconductivity in Si has also been achieved in gallium enriched Si layers (Ga:Si) by rapid thermal annealing of gallium ion implanted Si<sup>1</sup> and also by doping boron in Si (B:Si) above the equilibrium solubility by using gas immersion laser doping.<sup>2,3</sup> In a recent article, Shim et. al<sup>4</sup> proposed the idea of fabricating superconducting circuits and Josephson junctions in a group-IV semiconductor. Realization of this proposal primarily depends on successful realization of superconductivity in a semiconductor. Despite the higher critical temperature ( $T_c = 7$  K) of the Ga:Si,<sup>1</sup> the material system may not be ideal for quantum information processing device fabrication as the superconducting regions lie at the Si-SiO<sub>2</sub> interface.<sup>1</sup> The  $T_c$  of the B:Si systems is approximately 0.35 K,<sup>2</sup> but an Al:Si system is predicted to have an order of magnitude higher  $T_c$  compared to B:Si.<sup>5</sup>

Semiconducting p-type delta-layers in a Si/Al/Si heterostructure can also shed light on other interesting scientific and technological areas. For instance, as a result of longer spin decoherence times due to the suppression of hyperfine interaction between holes and nuclear spins,<sup>6</sup> hole-based qubit design has attracted significant interest<sup>7,8</sup> within semiconductor quantum information processing (qubit) device architectures. Stronger spin-orbit coupling in a hole-based spin qubit will enable the realization of all-electrical spin manipulation.<sup>9,10</sup> Moreover, hole spin qubits in Si can also benefit from the absence of valley degeneracy that complicate the electrical properties in electron based qubits.

<sup>a</sup>Correspondence to [joshua.pomeroy@nist.gov](mailto:joshua.pomeroy@nist.gov)

Also, p-type delta doping in combination with atomically abrupt interfaces to n-type delta doping in Si can open new avenues for realizing new transistor mechanisms that offer substantial energy reductions in switching applications along with short gate lengths and low leakage.<sup>11</sup> To reach atomically abrupt interfaces and the ultimate goal of single atom placement and measurement, new MBE (molecular beam epitaxy) techniques have been developed that allow the formation of “delta” layers.<sup>12–16</sup> The delta layer refers to the formation of a two dimensional doped region embedded in Si, whose effective thickness is similar to the electronic Bohr radius of the dopant in Si, resulting in the electronic structure having a two-dimensional form. Despite the success of the phosphine dosing of Si(100) surface and subsequent epitaxial overgrowth,<sup>17–20</sup> to create n-type dopant layers with atomically abrupt interfaces, a complementary p-type system is yet to emerge.

Therefore, our realization of a p-type delta-doped Si/Al/Si heterostructure can benefit a variety of research disciplines. New opportunities emerge when both semiconducting and superconducting properties exist in the same crystalline Si without a different material interface. Here we report the realization of a quasi two dimensional (2D) hole system formed from a monolayer of Al in Si. The material properties are characterized using STM (scanning tunneling microscopy), APT (atom probe tomography), STEM (scanning transmission electron microscopy), and the electrical properties are evaluated by low temperature transport measurements on multi-terminal Hall bar devices.

Synthesis of Al delta layers sandwiched in Si (see Fig. 1a) is carried out in a dedicated ultra high vacuum (UHV) system with base pressure less than  $7 \times 10^{-9}$  Pa ( $<5 \times 10^{-11}$  Torr). First, high resistivity ( $\rho > 10$  k $\Omega$ ) Si(100) samples (10 mm  $\times$  4 mm) were cleaned by using a standard RCA cleaning procedure.<sup>21</sup> The freshly cleaned Si chips were loaded into the UHV system and degassed at 600 °C for  $> 8$  h. The Si samples were flash annealed<sup>22</sup> at  $\approx 1200$  °C to achieve a pristine (2  $\times$  1) reconstructed Si(100) surface. Upon inspecting the with the STM, the sample was subjected to another brief flash anneal at  $\approx 1200$  °C clean any contamination introduced by STM prior to depositing Al by means of thermal evaporation. The Al evaporation rate was determined by analyzing the STM images of samples at low Al coverage. After Al deposition, the sample is again investigated with STM and, as shown in Fig. 1b, a (2  $\times$  2) reconstruction of Al atoms on Si(100) can be seen indicating good crystal structure and coverage of Al atoms. The 2D density of Si atoms in Si(100) surface is

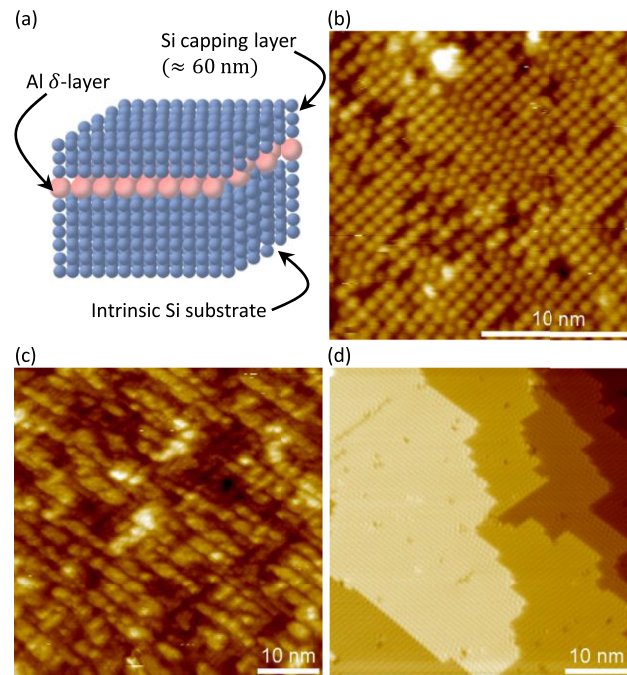


FIG. 1. (a) Schematic of the Al delta layer sandwiched in Si is shown. STM topography images of (b) as-deposited Al monolayer on the Si(100) surface, (c) Si (100) surface after Al incorporation, and (d) Si surface after overgrowth and recrystallization are shown.

$6.78 \times 10^{14} \text{ cm}^{-2}$ ;<sup>23</sup> therefore, the maximum number of Al atoms that can be put down on a Si(100) surface is  $\approx 1.69 \times 10^{14} \text{ cm}^{-2}$ . i.e., total number of Al atoms in a monolayer (ML) of Al on Si(100) surface is equivalent to 25 % of Si atoms in a Si(100) surface. For the devices reported here, by counting the number of Al atoms on the STM images (see Fig. 1b), we estimate that we have deposited one ML of Al covering  $(89 \pm 10) \%$  of the Si(100) surface, i.e., the total number of Al atoms deposited is  $\approx (1.5 \pm 0.2) \times 10^{14} \text{ cm}^{-2}$ , at room temperature in UHV. Here the uncertainty in Al coverage is largely due to the uncertainty in counting and the uncertainty in determining the length scale of the STM image. The sample is then subjected to an anneal at  $550 \text{ }^\circ\text{C}$  for 1 min to incorporate Al into the Si lattice (see Fig. 1c) followed by  $\approx 60 \text{ nm}$  Si overgrowth at room temperature at a rate of approximately 1 ML/min to 1.2 ML/min. Finally the dopants were activated by annealing the sample at  $550 \text{ }^\circ\text{C}$  for 10 min in UHV. This  $550 \text{ }^\circ\text{C}$  anneal also helps to reconstruct the Si capping layer to improve the crystallinity. As shown in Fig. 1d, the overgrown Si demonstrates the expected  $2 \times 1$  surface reconstruction for Si(100).

To characterize the electrical properties, synthesized Al delta layer specimens were mesa etched into multi-terminal Hall bar devices ( $50 \mu\text{m} \times 1000 \mu\text{m}$ ) (see Fig. 2a). First, the Hall bar devices were photolithographically patterned and mesa etched ( $\approx 100 \text{ nm}$ ) in an oxygen plasma in a reactive ion etching (RIE) chamber. Metal contacts were then defined by using sputter deposited Al metal ( $\approx 300 \text{ nm}$ ) followed by photolithographic patterning and a wet etch process. Finally, upon stripping the photoresist, the samples were subjected to a RTA (rapid thermal anneal) at  $350 \text{ }^\circ\text{C}$  for 30 min to improve the electrical connection between the buried delta layer and the Al metal contacts.

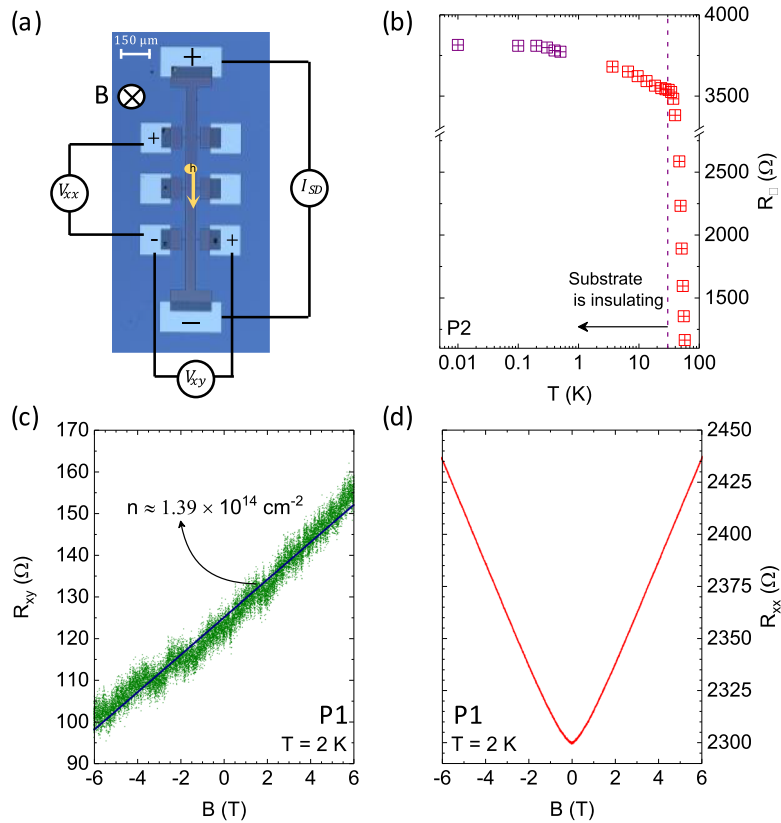


FIG. 2. (a) Micrograph of the  $50 \mu\text{m}$  wide mesa etched Hall bar device, and schematic of the measurement circuit is shown. Externally applied magnetic field ( $B$ ) is pointing into the plane of the substrate and the arrow (yellow) shows the direction of the flow of the holes (current). (b) Resistance per square ( $R_{\square}$ ) as a function of the temperature ( $T$ ) down to  $10 \text{ mK}$  is shown for sample P2. For  $T \geq 30 \text{ K}$  the substrate is conducting. Below  $30 \text{ K}$  the substrate is insulating and the delta layer reaches a finite resistance. (c) The Hall resistance ( $R_{xy}$ ) and (d) the magnetoresistance ( $R_{xx}$ ) are shown for sample P1 at  $T = 2 \text{ K}$ .

Resistance per-square ( $R_{\square}$ ) versus temperature ( $T$ ) for a Hall bar device (P2) fabricated on Al delta layer material is shown in Fig. 2b. Higher temperature ( $T \geq 3$  K) data were measured in a closed cycle refrigerator, while warming up the system and low temperature ( $T \leq 3$  K) data were measured in a cryogen free dilution refrigerator (DR). The sample P2 did not exhibit superconductivity down to the base temperature ( $T = 10$  mK) of the DR. Based on separate measurements (not discussed here), we estimate that the actual electron temperature of the device was  $\approx 300$  mK when the DR was at its base temperature.

Magnetoresistance ( $R_{xx}$ ) and Hall resistance ( $R_{xy}$ ) measured on sample P1 are shown in Fig. 2c and d. The measurements reported here were done with a DC current bias across the Hall device. As shown in the schematic of Fig. 2a, the positive slope of  $R_{xy}$  indicates that the dominant charge carriers contributing to the transport are in fact holes. Charge carrier density ( $n_h$ ) and the mobility ( $\mu$ ) extracted using  $R_{xy}$  and  $R_{xx}$  data are  $\approx 1.39 \times 10^{14}$  cm $^{-2}$  and  $\approx 20$  cm $^2$ /(Vs), respectively at  $T = 2$  K. The mobility for our Al:Si is comparable to mobilities reported for B:Si at similar densities.<sup>24</sup> The relative uncertainties for both  $n_h$  and  $\mu$  are less than 1 %. The extracted charge carrier density corresponds to approximately  $(0.93 \pm 0.1)$  hole per Al dopant atom.

$R_{xx}$  at different temperatures is shown in Fig. 3a. At low  $B$  fields ( $B < 1$  T),  $R_{xx}$  demonstrates fairly standard parabolic behavior<sup>25</sup> except for near zero  $B$  field. At low  $T$ , and near zero  $B$  field,  $R_{xx}$  deviates from a parabolic nature and demonstrates an anomalous behavior similar to weak-antilocalization,<sup>26</sup> see Fig. 3a inset. Here for  $|B| \leq 2$  T,  $\delta R_{xx}$  is defined as  $\delta R_{xx} = R_{xx}(B) - R_{bkg}$  and  $R_{bkg} = R_0 + A \times B^2$ , where  $B$  is the applied magnetic field,  $R_0$  is the resistance at  $B = 0$ , and  $A$  is a constant. The weak-antilocalization-like feature diminishes with increasing temperature and disappears around  $T = 14$  K (Fig. 3a inset). The inelastic scattering time ( $\tau_{in}$ ) typically increases at low temperatures as

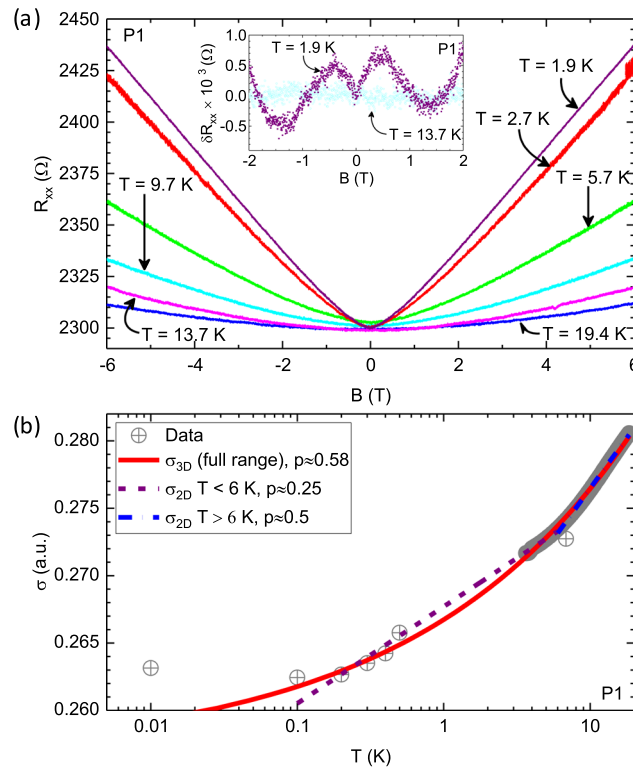


FIG. 3. (a) Magnetoresistance ( $R_{xx}$ ) data measured at temperatures from 1.9 K to 19.4 K are shown for sample P1. At higher magnetic fields  $R_{xx}$  becomes linear in  $B$  for temperatures 5.7 K, 2.7 K, and 1.9 K. Inset: A parabolic background subtracted from  $R_{xx}$  ( $\delta R_{xx}$ ) is shown for temperatures 1.9 K and 13.7 K. At low temperatures near zero  $B$  field,  $R_{xx}$  shows a behavior similar to weak-antilocalization. (b) Conductivity,  $\sigma = 1/\rho_{xx} \propto 1/R_{xx}(B = 0)$ , versus temperature is shown and compared with the behavior of a weakly localized system. The temperature reported here is the fridge thermometer temperature, and the fits were done for  $T > 200$  mK.

$\tau_{in} \propto T^{-p}$ ; therefore, the dephasing length ( $L_{th}$ ) becomes temperature dependent as  $L_{th} \propto \sqrt{\tau_{in}}$ . The value index  $p$  depends upon the dominant scattering mechanism, as well as the dimensionality of the conduction channel.<sup>27</sup> The scale dependent localization effects are limited to this length scale  $L_{th}$ , and therefore we are using the dependence of conductivity in temperature to deduce the dimensionality of the conduction channel. Figure 3b shows the variation of  $\sigma = 1/\rho_{xx} \propto 1/R_{xx}$  with temperature at  $B = 0$ . When we consider the entire temperature range, the data agree well with the extended conductance variation of a three-dimensional (3D) conduction channel, where  $\sigma_{3D}(T) = \sigma_0 + T^{p/2} e^2/(\hbar\pi^3 a)$ ,<sup>27</sup> which yields  $p = 0.58 \pm 0.07$ . Here  $a$  is associated with the dimensionality of the conduction channel,  $\sigma_0$  is the Boltzmann transport conductivity. We can also fit the data to a model assuming a two-dimensional (2D) conduction channel, where  $\sigma_{2D}(T) = \sigma_0 + p e^2/(2\hbar\pi^2) \ln(T/T_0)$ .<sup>27</sup> The 2D model does not fit well for the entire temperature range, but can be fit to the low temperatures ( $T < 6$  K) and high temperatures ( $T > 6$  K) regimes separately. The fits yield  $p = 0.25$  and  $p = 0.53$  for lower and higher temperature regimes, respectively. The relative uncertainty in  $p$  for 2D model is  $< 1\%$ . Neither of these values of  $p$  correspond to the expected value for a weakly localized 2D system. Therefore, the analysis of conductance versus the temperature suggests that the Al dopants have diffused over a finite width creating a 3D (quasi-2D) conduction channel.

We also note that at lower temperatures ( $T < 6$  K),  $R_{xx}$  becomes linear in  $B$ , especially at higher  $B$  fields, i.e.,  $B > 1$  T. This deviation from parabolic to linear  $R_{xx}$  occurs around the same temperature where the value of  $p$  changes from approximately 0.5 to 0.25 for  $\sigma_{2D}$ . The linear magnetoresistance (LMR) can be due to polycrystallinity<sup>28,29</sup> or topological effects.<sup>30,31</sup> Aside from these, a strong field, non saturating LMR is also proposed for crystals with inhomogeneities.<sup>32</sup> Polycrystallinity and inhomogeneities in the material (inhomogeneities in distribution of Al dopants) are possible candidates for observed LMR.

To explore possible reasons for not observing superconductivity, we examine the distribution of the Al delta layer material using APT, and STEM by preparing cross-sectional samples from device P1. APT samples were prepared directly under an Al electrical contact pad; therefore, a background has been subtracted to account for the Al diffused downward during the metal contact anneal. The resulting Al profile is shown in Fig. 4a, and on average APT extracted Al atom density is approximately  $(1.2 \pm 0.3) \times 10^{14} \text{ cm}^{-2}$ , and shows that Al dopants have distributed over a width of

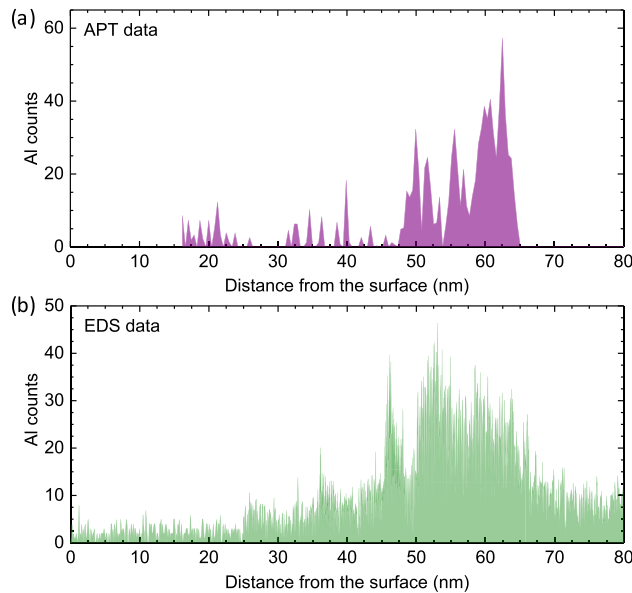


FIG. 4. Al distribution as determined by (a) APT, and (b) the sum of 5 STEM-EDS scans from sample P1 is shown. According to APT, the Al monolayer has diffused over approximately 17 nm width. The average number of Al atoms that APT data account for is approximately  $(1.2 \pm 0.3) \times 10^{14} \text{ cm}^{-2}$ . STEM-EDS data also confirm the diffusion of Al dopant over a similar range ( $\approx 25$  nm). The uncertainty in position between APT and EDS data is approximately  $\pm 10$  nm. For both the graphs the surface is at zero thickness.

$\approx 17$  nm. Even though the numbers agree within the uncertainties, we believe the apparent decrease of the average Al density in APT data compared to the STM estimation is due to the difficulty in properly modeling the background in the APT concentration profile. The STEM-EDS (energy-dispersive X-ray spectroscopy) profile of the Al taken from another part of the specimen (see Fig. 4b) also confirms a similar distribution of Al dopants over a width of  $\approx 25$  nm.

Preliminary STEM (data not shown) analyses confirm that the Si is crystalline near the Al enriched region; therefore, polycrystallinity causing the observed LMR is highly unlikely. However, the 3D reconstruction of APT data (not shown) seem to indicate local concentration variations in the Al along the Al:Si region. Therefore, we believe that an inhomogeneous distribution of Al dopants is the reason for observation of LMR.

According to the APT (STEM-EDS) data and assuming a 2D density of Al atoms to be  $\approx 1.5 \times 10^{14} \text{ cm}^{-2}$  (maximum density of Al atoms according to STM analysis), we estimate an upper bound for 3D density of Al atoms in Si to be approximately 0.2 % (0.1 %). But the estimated 3D density of Al in these samples, considering APT data, is only approximately a tenth of what is predicted to observe superconductivity in B:Si heterostructure assuming similar conditions apply for Al:Si.<sup>3</sup> The diffusion of Al is also consistent with the low temperature electrical measurements indicating a 3D conduction channel contributing to electrical transport. Therefore, we argue that even though we started with a higher 2D density of Al atoms  $\approx 1.5 \times 10^{14} \text{ cm}^{-2}$ , the final 3D Al density falling below the critical density predicted for superconductivity due to re-distribution as the dominant reason for not observing superconductivity in these samples.

Calculation of diffusion length ( $L$ ) of Al in bulk crystalline Si, where  $L = \sqrt{Dt}$  and  $D = D_0 e^{-E_a/k_B T}$ , indicate that Al should have diffused  $< 1$  nm upon annealing at  $550^\circ\text{C}$  for 10 min, for prefactor  $D_0 = 4.73 \text{ cm}^2/\text{s}$  and activation energy  $E_a = 3.35 \text{ eV}$ .<sup>33</sup> Here  $D$ ,  $E_a$ ,  $k_B$  are the diffusion coefficient, activation energy, and Boltzmann constant, respectively. However, it is also important to note that for this material, room temperature Si overgrowth is likely amorphous (or polycrystalline) prior to the  $550^\circ\text{C}$  anneal. Therefore, the values of  $D_0$  and  $E_a$  can vary significantly based on the quality of Si<sup>34</sup> causing the Al dopants to diffuse more into the overgrown Si capping layer. The targeted thickness of the capping layer is approximately  $(60 \pm 10)$  nm; therefore, the abrupt decrease in the Al profile near 65 nm mark is consistent with targeted capping layer thickness and negligible Al diffusion into Si substrate. In the future, we believe that by increasing the growth temperature (e.g.  $350^\circ\text{C}$ ) of the capping layer, we can achieve crystallinity in the overgrown Si layer, and can constrain the Al dopants to a narrower region to achieve a higher 3D density of Al in Si.

In conclusion, we have successfully synthesized a quasi two-dimensional hole gas in Si by using a monolayer of Al sandwiched in Si. Resistance measured as a function of temperature does not show signs of superconductivity. The redistribution of Al dopants over approximately 17 nm (according to APT data) have reduced the 3D Al density to only 10 % of the predicted density to observe superconductivity in B:Si assuming similar conditions apply for Al:Si. We believe this dopant diffusion is the root cause for not observing superconductivity in these devices. We plan future experiments on parameters such as Si overgrowth temperature and annealing temperature to reduce the Al distribution width and increase the 3D Al density.

The authors acknowledge stimulating discussions with Michael Stewart, Ryan Stein, Binhui Hu, Peihao Huang. H. Z. acknowledges support from the U.S. DOC, NIST under the financial assistance awards 70NANB15H025 and 70NANB17H249. This work was performed in part at the Center for Nanoscale Science and Technology.

<sup>1</sup>R. Skrotzki, J. Fiedler, T. Herrmannsdörfer, V. Heera, M. Voelskow, A. Mücklich, B. Schmidt, W. Skorupa, G. Gobsch, M. Helm, and J. Wosnitza, "On-chip superconductivity via gallium overdoping of silicon," *Applied Physics Letters* **97**, 192505 (2010).

<sup>2</sup>E. Bustarret, C. Marcenat, P. Achatz, J. Kačmarčík, F. Lévy, A. Huxley, L. Ortéga, E. Bourgeois, X. Blase, D. Débarre, and J. Boulmer, "Superconductivity in doped cubic silicon," *Nature* **444**, 465 (2006).

<sup>3</sup>C. Marcenat, J. Kačmarčík, R. Piquerel, P. Achatz, G. Prudon, C. Dubois, B. Gautier, J. C. Dupuy, E. Bustarret, L. Ortéga, T. Klein, J. Boulmer, T. Kociniowski, and D. Débarre, "Low-temperature transition to a superconducting phase in boron-doped silicon films grown on (001)-oriented silicon wafers," *Phys. Rev. B* **81**, 020501 (2010).

<sup>4</sup>Y.-P. Shim and C. Tahan, "Bottom-up superconducting and josephson junction devices inside a group-iv semiconductor," *Nature Communications* **5**, 4225 (2014).

- <sup>5</sup> E. Bourgeois and X. Blase, "Superconductivity in doped cubic silicon: An ab initio study," *Applied Physics Letters* **90**, 142511 (2007).
- <sup>6</sup> Z. K. Keane, M. C. Godfrey, J. C. H. Chen, S. Fricke, O. Klochan, A. M. Burke, A. P. Micolich, H. E. Beere, D. A. Ritchie, K. V. Trunov, D. Reuter, A. D. Wieck, and A. R. Hamilton, "Resistively detected nuclear magnetic resonance in n- and p-type GaAs quantum point contacts," *Nano Letters* **11**, 3147–3150 (2011).
- <sup>7</sup> D. V. Bulaev and D. Loss, "Spin relaxation and decoherence of holes in quantum dots," *Phys. Rev. Lett.* **95**, 076805 (2005).
- <sup>8</sup> B. D. Gerardot, D. Brunner, P. A. Dalgarno, P. Öhberg, S. Seidl, M. Kroner, K. Karrai, N. G. Stoltz, P. M. Petroff, and R. J. Warburton, "Optical pumping of a single hole spin in a quantum dot," *Nature* **451**, 441 (2008).
- <sup>9</sup> P. Szumniak, S. Bednarek, B. Partoens, and F. M. Peeters, "Spin-orbit-mediated manipulation of heavy-hole spin qubits in gated semiconductor nanodevices," *Phys. Rev. Lett.* **109**, 107201 (2012).
- <sup>10</sup> J.-T. Hung, E. Marcellina, B. Wang, A. R. Hamilton, and D. Culcer, "Spin blockade in hole quantum dots: Tuning exchange electrically and probing Zeeman interactions," *Phys. Rev. B* **95**, 195316 (2017).
- <sup>11</sup> S. Agarwal and E. Yablonoivitch, "Pronounced effect of pn-junction dimensionality on tunnel switch threshold shape," [arXiv:1109.0096](https://arxiv.org/abs/1109.0096).
- <sup>12</sup> H.-J. Gossmann, F. Unterwald, and H. Luftman, "Doping of Si thin films by low-temperature molecular beam epitaxy," *Journal of Applied Physics* **73**, 8237–8241 (1993).
- <sup>13</sup> H.-J. Gossmann, E. Schubert, D. Eaglesham, and M. Cerullo, "Low-temperature Si molecular beam epitaxy: Solution to the doping problem," *Applied Physics Letters* **57**, 2440–2442 (1990).
- <sup>14</sup> K. J. Dwyer, H. S. Kim, D. S. Simons, and J. M. Pomeroy, "Temperature-dependent Si incorporation during deposition of highly enriched Si 28 films," *Physical Review Materials* **1**, 064603 (2017).
- <sup>15</sup> D. Eaglesham, "Semiconductor molecular-beam epitaxy at low temperatures," *Journal of Applied Physics* **77**, 3597–3617 (1995).
- <sup>16</sup> S. R. McKibbin, W. R. Clarke, and M. Y. Simmons, "Investigating the surface quality and confinement of Si: P  $\delta$ -layers at different growth temperatures," *Physica E: Low-Dimensional Systems and Nanostructures* **42**, 1180–1183 (2010).
- <sup>17</sup> S. McKibbin, C. Polley, G. Scappucci, J. Keizer, and M. Simmons, "Low resistivity, super-saturation phosphorus-in-silicon monolayer doping," *Applied Physics Letters* **104**, 123502 (2014).
- <sup>18</sup> M. Fuechle, J. A. Miwa, S. Mahapatra, H. Ryu, S. Lee, O. Warschkow, L. C. Hollenberg, G. Klimeck, and M. Y. Simmons, "A single-atom transistor," *Nature Nanotechnology* **7**, 242 (2012).
- <sup>19</sup> B. Weber, S. Mahapatra, H. Ryu, S. Lee, A. Fuhrer, T. Reusch, D. Thompson, W. Lee, G. Klimeck, L. C. Hollenberg *et al.*, "Ohm's law survives to the atomic scale," *Science* **335**, 64–67 (2012).
- <sup>20</sup> J. A. Hagmann, X. Wang, P. Nambodiri, J. Wyrick, R. Murray, M. Stewart, Jr., R. M. Silver, and C. A. Richter, "High resolution thickness measurements of ultrathin Si: P monolayers using weak localization," *Applied Physics Letters* **112**, 043102 (2018).
- <sup>21</sup> W. Kern, *Semicond. Int.* **7**, 94 (1984).
- <sup>22</sup> A. N. Ramanayaka, H.-S. Kim, K. Tang, X. Wang, R. M. Silver, M. D. Stewart, and J. M. Pomeroy, "STM patterned nanowire measurements using photolithographically defined implants in Si(100)," *Scientific Reports* **8**, 1790 (2018).
- <sup>23</sup> E. G. Keim, L. Wolterbeek, and A. V. Silfhout, "Adsorption of atomic oxygen (n<sub>2</sub>O) on a clean Si(100) surface and its influence on the surface state density; a comparison with O<sub>2</sub>," *Surface Science* **180**, 565–598 (1987).
- <sup>24</sup> H.-J. Gossmann and F. C. Unterwald, "Dopant electrical activity and majority-carrier mobility in b- and sb- $\delta$ -doped Si thin films," *Phys. Rev. B* **47**, 12618–12624 (1993).
- <sup>25</sup> A. Sommerfeld and N. H. Frank, "The statistical theory of thermoelectric, galvanic- and thermomagnetic phenomena in metals," *Rev. Mod. Phys.* **3**, 1–42 (1931).
- <sup>26</sup> G. Bergmann, "Weak localization in thin films: a time-of-flight experiment with conduction electrons," *Physics Reports* **107**, 1–58 (1984).
- <sup>27</sup> P. A. Lee and T. V. Ramakrishnan, "Disordered electronic systems," *Rev. Mod. Phys.* **57**, 287–337 (1985).
- <sup>28</sup> P. Kapitza, "The study of the specific resistance of bismuth crystals and its change in strong magnetic fields and some allied problems," *Proceedings of the Royal Society of London A: Mathematical, Physical and Engineering Sciences* **119**, 358–443 (1928).
- <sup>29</sup> A. A. Abrikosov, "Quantum linear magnetoresistance; solution of an old mystery," *Journal of Physics A: Mathematical and General* **36**, 9119 (2003).
- <sup>30</sup> M. Novak, S. Sasaki, K. Segawa, and Y. Ando, "Large linear magnetoresistance in the Dirac semimetal TlBiSe<sub>2</sub>," *Phys. Rev. B* **91**, 041203 (2015).
- <sup>31</sup> J. Tian, C. Chang, H. Cao, K. He, X. Ma, Q. Xue, and Y. P. Chen, "Quantum and classical magnetoresistance in ambipolar topological insulator transistors with gate-tunable bulk and surface conduction," *Scientific Reports* **4**, 4859 (2014).
- <sup>32</sup> A. B. Pippard, *Magnetoresistance in metals* (Cambridge University Press, 2009).
- <sup>33</sup> O. Krause, H. Ryssele, and P. Pichler, "Determination of aluminum diffusion parameters in silicon," *Journal of Applied Physics* **91**, 5645–5649 (2002).
- <sup>34</sup> J. C. M. Hwang, P. S. Ho, J. E. Lewis, and D. R. Campbell, "Grain boundary diffusion of aluminum in polycrystalline silicon films," *Journal of Applied Physics* **51**, 1576–1581 (1980).